Trial application of the envelope method to the potential ambiguity problem*

Liyuan Hu[1,2,3] and Yushou Song[1,2,3,†]

[1]*Fundamental Science on Nuclear Safety and Simulation Technology Laboratory, Harbin Engineering University, Harbin, 150001, China*
[2]*College of Nuclear Science and Technology, Harbin Engineering University, Harbin, 150001, China*
[3]*Key Laboratory of Nuclear Safety and Advanced Nuclear Energy Technology, Ministry of Industry and Information Technology, Harbin, 150001, China*

The optical potential ambiguity is a long-standing problem in the analysis of elastic scattering data.

For a specific colliding system, ambiguous potential families can lead to different behaviors in the nearside and farside scattering components.

By contrast, the envelope method can decompose the experimental data into two components with negative and positive deflection angles, respectively. Hence, a question arises as to whether the comparison between the calculated nearside (or farside) component and the derived positive-deflection-angle (or negative-deflection-angle) component can help analyze the potential ambiguity problem. In this study, we conducted a trial application of the envelope method to the potential ambiguity problem. The envelope method was improved by including uncertainties in the experimental data.

The colliding systems of ^{16}O+^{28}Si at 215.2 MeV and ^{12}C+^{12}C at 1016 MeV were considered in the analyses. For each colliding system, the angular distribution experimental data were described nearly equally well by two potential sets, one of which is "surface transparent" and the other is refractive. The calculated angular distributions were decomposed into nearside and farside scattering components. Using the improved envelope method, the experimental data were decomposed into the positive-deflection-angle and negative-deflection-angle components, which were then compared with the calculated nearside and farside components. The capability of the envelope method to analyze the potential ambiguities was also discussed.

Keywords: elastic scattering, optical potential ambiguities, envelope method, nearside/farside decomposition

I. INTRODUCTION

Optical potential represents the interaction between colliding nuclei pairs and plays an important role in the analyses of nuclear reactions [1]. The parameters of empirical optical potentials are typically obtained by fitting the experimental data of elastic scattering angular distributions (e.g., Refs. [2–5]). However, the ambiguity problem usually exists in the obtained potential parameters, which implies that the experimental data can be fitted equally well to different sets of potential parameters [1]. Potential ambiguities can be classified into several different types, including continuous, discrete, refractive or diffractive, and shallow- or deep-W ones, which have been investigated in many studies (e.g., Refs. [6–10]). Clearly, the ambiguity introduces problems in analyzing the reaction mechanisms [11–15]. Therefore, proper treatment is required to resolve the ambiguity problem and obtain more physical optical potentials. One approach is to use global energy-dependent optical potentials (such as those in Refs. [16–26]) to constrain the potential parameters. In addition, for the elastic scattering of two light heavy-ion systems, it was found that the refractive farside scattering data can help eliminate the discrete and shallow- or deep-W ambiguities [1].

In Ref. [10], Hussein and McVoy highlighted that at energies well above the Coulomb barrier, the nearside and farside scattering components exhibit different behaviors for the refractive and diffractive optical potentials. For the refractive potential, the nearside scattering component shows a larger slope than the farside component (when using $\ln(d\sigma/d\theta)$ as the vertical coordinate). Consequently, the two components can construct the localized Fraunhofer crossover point, and a deep minimum appears near the corresponding scattering angle in the total differential cross sections. However, for the diffractive potential, the nearside and farside components are nearly parallel. In this case, rather than the localized Fraunhofer crossover point, a much wider Fraunhofer oscillation structure exists. The authors of Ref. [10] have taken the elastic scattering of ^{16}O+^{28}Si at 215.2 MeV as an example to show the differences between the nearside/farside decompositions calculated with the refractive potential and the diffractive one. For this colliding system, both the refractive deep-V potential called "A-type" potential and the diffractive shallow-V potential called "E18" potential (which is also known as "surface transparent") can effectively reproduce the existing experimental data of the angular distribution [9]. However, the nearside and farside scattering components calculated using the two types of optical potentials exhibit different behaviors. For the nearside components, the difference in slopes is significantly small at angles smaller than those at which the nearside and farside components are close to each other. However, at larger angles, the nearside component calculated with the "E18" potential shows a relatively smaller slope than the one calculated with the "A-type" potential. For the farside scattering, different from the nearside case, the calculated cross sections with the "A-type" potential shows a smaller slope than that calculated with the "E18" potential in the whole angular range. These results

* This work was supported by the National Natural Science Foundation of China (Grant Nos. 12005047 and U1832105).
† Corresponding authorsongyushou80@163.com

indicate that a comparison between the nearside and/or farside components can be used to demonstrate the differences between the ambiguous potential families.

In Ref. [27], da Silveira and Leclercq-Willain proposed an envelope method to decompose the experimental data of the elastic scattering angular distribution into two scattering components with negative and positive deflection angles, respectively. In this method, two envelopes were drawn for the experimental data with the well-defined maxima and minima in the data. Moreover, "experimental" data points corresponding to the negative- and positive-deflection-angle components can be derived. In Ref. [27], this method was applied to the elastic scattering data of α+^{40}Ca at 104 MeV and α+^{58}Ni at 140 MeV without considering the uncertainties introduced by the experimental data. In addition, this method has been extended to investigate the refractive phase relationship between elastic and inelastic scattering and the decomposition of the farside scattering angular distribution [28, 29]. In Ref. [30], the experimental dataset of α+^{40}Ca at 104 MeV was further analyzed using the envelope method. The obtained differential cross-section data of the positive- and negative-deflection-angle components agree well with the nearside and farside scattering components, respectively. Combined with the behaviors of nearside and farside scattering mentioned above, our observations inspired us to consider the envelope method as a potential solution to address the ambiguity problem. This could be achieved by comparing the "experimental" positive- and negative-deflection-angle components with the theoretical nearside and farside components, respectively.

In this study, a trial application of the envelope method to the potential ambiguity problem was performed. The experimental data of the elastic scattering angular distributions of ^{16}O+^{28}Si at 215.2 MeV and ^{12}C+^{12}C at 1016 MeV were selected, and the optical potential ambiguity between the "surface transparent" and refractive potentials were studied. Optical model calculations and corresponding nearside/farside decompositions were performed for each dataset. Using the envelope method, the experimental data points within the angular range covered by the well-defined maxima and minima were decomposed into positive- and negative-deflection-angle cross-section components. To estimate the uncertainty of the two components, the errors of the experimental data points used in the construction of the envelopes were considered. The capability of the envelope method to analyze the potential ambiguity problem was discussed by comparing the obtained positive/negative-deflection-angle cross-sectional components with the calculated results of the nearside/farside decompositions.

II. METHOD

The optical model, the nearside/farside decomposition and the envelope methods were utilized to analyze the experimental data. In this section, the latter two methods are briefly outlined; more details can be found in Ref. [27, 30–33].

In the envelope method, the starting point is a partial-wave expansion of the scattering amplitude [27]. Using the asymptotic expression of the Legendre polynomials, the scattering amplitude can be decomposed into the components corresponding to the positive and negative deflection angles, which are denoted by $f_+(\theta)$ and $f_-(\theta)$, respectively.

$$f(\theta) = f_+(\theta) + f_-(\theta). \tag{1}$$

In the classical limit, $f_+(\theta)$ and $f_-(\theta)$ can be expressed as follows [30]:

$$f_\pm(\theta) = \frac{1}{ik(2\pi\sin\theta)^{1/2}} \sum_{l=0}^{\infty} \left(l+\frac{1}{2}\right)^{1/2} e^{i\left[2\delta_l \mp \left(l+\frac{1}{2}\right)\theta \pm \frac{1}{4}\pi\right]}. \tag{2}$$

where δ_l is the nuclear plus the Coulomb phase shift. The cross sections corresponding to the positive and negative deflection angles are denoted as $\sigma_+(\theta)$ and $\sigma_-(\theta)$, respectively, which are related to the scattering amplitudes as follows:

$$\sigma_\pm(\theta) = |f_\pm(\theta)|^2. \tag{3}$$

It should be noted that the signs ("+" and "−") used as subscript are similar to those used in Ref. [30] but in contrast to those used in Ref. [27]. The elastic scattering angular distribution $\sigma(\theta)$=$|f(\theta)|^2$ oscillates between the upper envelope E_u and lower envelope E_l defined by

$$E_u(\theta) = \left(\sigma_+^{1/2}(\theta) + \sigma_-^{1/2}(\theta)\right)^2, \tag{4}$$

and

$$E_l(\theta) = \left(\sigma_+^{1/2}(\theta) - \sigma_-^{1/2}(\theta)\right)^2. \tag{5}$$

According to Eq. (4) and (5), the positive- and negative-deflection-angle scattering cross sections can be obtained using two envelopes of the experimental elastic scattering angular distribution. The upper and lower envelopes are determined by the maxima and minima of the angular distribution, respectively. The envelopes can be drawn if the maxima and minima are well-defined in the experimental angular distribution. In the present study, the envelopes were drawn by connecting these maxima and minima with broken lines. The broken lines were then smoothed using the TGraph class provided by the ROOT software [34].

Observing Eq. (4) and (5), one can find that $\sigma_+(\theta)$ and $\sigma_-(\theta)$ follow the same relationship. Additional analysis is required to determine whether the solution obtained is $\sigma_+(\theta)$ or $\sigma_-(\theta)$. This problem can be resolved by observing the trends of the ratio of $\sigma_+(\theta)$ to the Rutherford scattering differential cross section $\sigma_R(\theta)$ because $\sigma_+(\theta)/\sigma_R(\theta)$ tends to unity as θ approaches zero and decreases almost exponentially as θ becomes larger [27, 30].

In previous studies based on the envelope method, uncertainties in the experimental data have not been considered quantitatively. For each maxima/minima data point, the mean value (μ) was used to determine the envelope. In the present work, in the construction of the envelopes, the standard deviation (dev) of each maxima/minima data point was also considered. In addition to μ, the envelopes were drawn for

$\mu + dev$ and $\mu - dev$ to estimate their uncertainties. Hence, there were three upper and three lower envelopes. The mean values of $\sigma_{\pm}(\theta)$ were obtained by combining the upper and lower μ envelopes. The other combinations of upper and lower envelopes were used to limit $\sigma_{+}(\theta)$ and $\sigma_{-}(\theta)$. Using this approach, the uncertainties can be propagated to the calculated $\sigma_{\pm}(\theta)$, which makes the envelope method more quantitative.

The nearside/farside decomposition of the scattering amplitude was performed using the method proposed by Fuller [31]. The scattering amplitude can be expressed as

$$f(\theta) = f_n(\theta) + f_f(\theta). \tag{6}$$

where $f_n(\theta)$ is the nearside scattering amplitude:

$$f_n(\theta) = \frac{1}{2ik}\sum_{l=0}^{\infty}(2l+1)[e^{2i\delta_l} - e^{2i\sigma_l}]Q_l^{(-)}(\cos\theta) + f_{C,n}(\theta), \tag{7}$$

and $f_f(\theta)$ is the farside scattering amplitude:

$$f_f(\theta) = \frac{1}{2ik}\sum_{l=0}^{\infty}(2l+1)[e^{2i\delta_l} - e^{2i\sigma_l}]Q_l^{(+)}(\cos\theta) + f_{C,f}(\theta). \tag{8}$$

In Eq.(7) and Eq. (8), $f_{C,n}$ and $f_{C,f}$ are the nearside and farside Coulomb scattering amplitudes, respectively; k is the relative wave number; σ_l is the Coulomb phase shift; and the travelling wave functions $Q_l^{(\pm)}(\cos\theta)$ are expressed as

$$Q_l^{(\pm)}(\cos\theta) = \frac{1}{2}[P_l(\cos\theta) \mp \frac{2i}{\pi}Q_l(\cos\theta)], \tag{9}$$

where $P_l(\cos\theta)$ and $Q_l(\cos\theta)$ are the Legendre functions of the first and second types of degree l, respectively. The differential cross sections corresponding to the nearside and farside scattering amplitudes are denoted as σ_n and σ_f, respectively:

$$\sigma_{n/f}(\theta) = |f_{n/f}(\theta)|^2. \tag{10}$$

In Ref. [30], it was shown that when $Q_l^{(\pm)}$ is replaced with asymptotic forms, f_n and f_f are simply amplitudes f_+ and f_-, respectively.

In the present work, the comparisons between "experimental" $\sigma_{\pm}(\theta)$ and the theoretical $\sigma_{n/f}(\theta)$ were performed to test the capability of the envelope method in treating the potential ambiguity problems. The optical model calculations were performed using FRESCO [35]. The nearside/farside decomposition was conducted according to the method described in Ref. [32].

III. RESULTS AND DISCUSSIONS

Experimental data for the elastic scattering angular distributions of ^{16}O+^{28}Si at 215.2 MeV (Ref. [36]) and ^{12}C+^{12}C at 1016 MeV (Ref. [37]) were analyzed using the optical model, the nearside/farside decomposition, and the envelope method, respectively.

TABLE 1. The nuclear optical potential parameters used in the optical model and nearside/farside decomposition calculations. The parameters for ^{16}O+^{28}Si at 215.2 MeV and ^{12}C+^{12}C at 1016 MeV are extracted from Ref. [9] and Ref. [11], respectively.

colliding system	potential set	V_0 (MeV)	$r_{\rm R}$ (fm)	$a_{\rm R}$ (fm)	W_0 (MeV)	$r_{\rm I}$ (fm)	$a_{\rm I}$ (fm)
^{16}O+^{28}Si	A1	10.00	1.350	0.618	23.40	1.230	0.552
	A2	100.00	0.967	0.745	44.10	1.073	0.850
^{12}C+^{12}C	B1	49.90	0.934	0.742	150.40	0.262	1.201
	B2	129.4	0.681	0.913	47.90	0.918	0.622

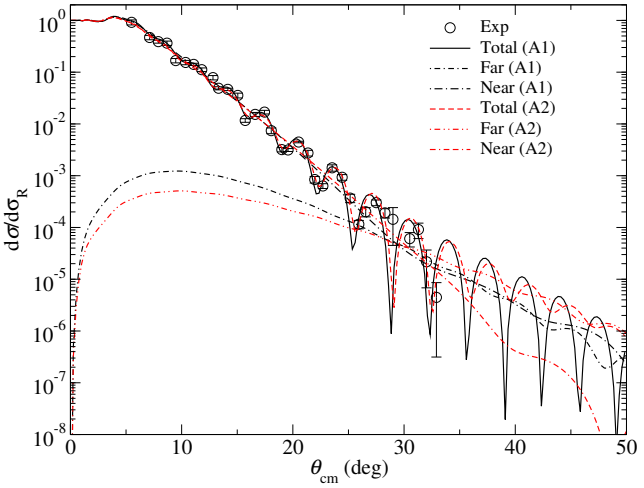

Fig. 1. Elastic scattering angular distribution of ^{16}O+^{28}Si at 215.2 MeV. The circles represent the experimental data. The curves are the results of the optical model and nearside/farside decomposition calculations with different potentials.

Experimental data for ^{16}O+^{28}Si at 215.2 MeV were obtained by digitizing the data points shown in "Fig. 6" in Ref. [38]. The digitizing software used in this study was GSYS (version 2.4.9) [39]. The experimental data for ^{12}C+^{12}C at 1016 MeV were obtained from the NRV database [40].

The optical potential parameters used in the optical model and the nearside/farside decomposition calculations are listed in Table 1. For both the systems, the "standard" Woods-Saxon function was adopted for the nuclear optical potentials:

$$U(r) = -\frac{V_0}{1+\exp\left(\frac{r-R_{\rm R}}{a_{\rm R}}\right)} - i\frac{W_0}{1+\exp\left(\frac{r-R_{\rm I}}{a_{\rm I}}\right)}, \tag{11}$$

where V_0 and W_0 are the depths of the real (R) and imaginary (I) parts, respectively. R_i and a_i ($i = R, I$) are the radius and diffuseness parameters, respectively. The reduced radius r_i (i=R, I) is defined as

$$r_i = R_i/(A_{\rm T}^{1/3} + A_{\rm P}^{1/3}),\ i = {\rm R, I} \tag{12}$$

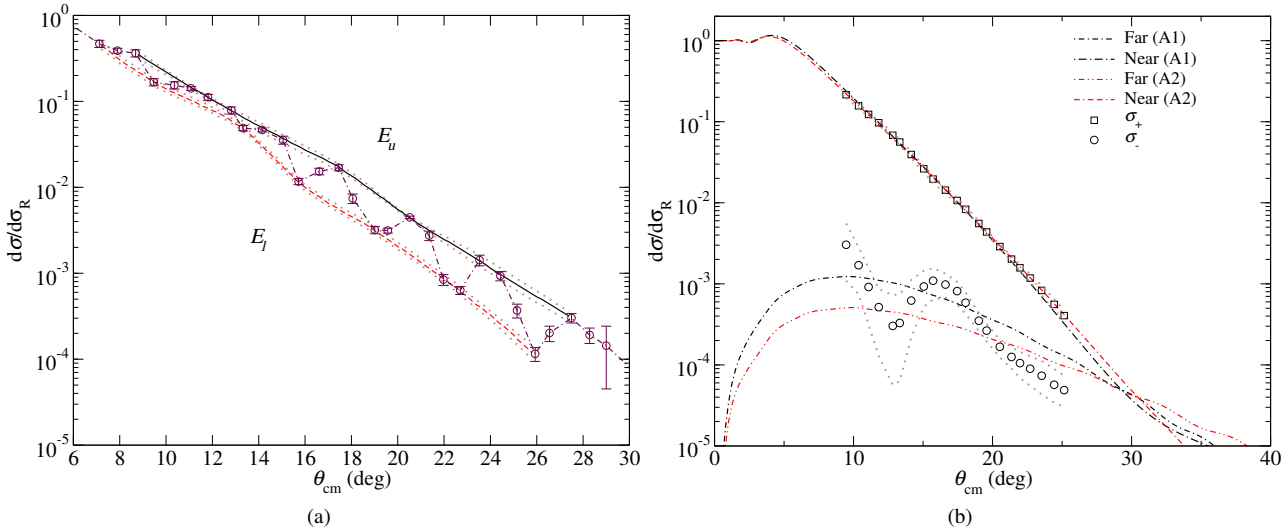

Fig. 2. Elastic scattering of ^{16}O+^{28}Si at 215.2 MeV: (a) envelopes of the experimental data; (b) greater/smaller components in comparison with the nearside/farside components.

where $A_{\rm T}$ and $A_{\rm P}$ are the atomic masses of the target and projectile, respectively. For the Coulomb potential, the potential between a point charge and a uniformly charged sphere was utilized. The optical potential parameters for ^{16}O+^{28}Si and ^{12}C+^{12}C were obtained from Ref. [9] and Ref. [11], respectively.

A. ^{16}O+^{28}Si at 215.2 MeV

First, we revisited the refractive or diffractive potential ambiguity problem of ^{16}O+^{28}Si at 215.2 MeV, as discussed in Ref. [9, 10]. In fact, the potential sets A1 and A2 are simply the diffractive shallow-V "E18" and refractive deep-V "A-type" ones, respectively [9]. The A1 potential is also a "surface transparent" potential, whose characteristic is a larger value of $R_{\rm R}$ than that of $R_{\rm I}$. Its real part is deeper than the imaginary part for $r > R_{\rm R}$ [10]. The results of the optical model and nearside/farside decomposition calculations are shown in Fig. 1. It can be seen that both the potential sets A1 and A2 can effectively reproduce the experimental data, although the theoretical angular distributions show quite different patterns at angles beyond approximately 35° where no data exist. As reported in Ref. [10], within the angular range covered by the experimental data, although the nearside components corresponding to A1 and A2 potentials are significantly close to each other, the farside components are evidently different.

The upper and lower envelopes of the experimental data are presented in Fig. 2(a). For each envelope, the uncertainties are represented by the region delimited by dotted lines. The positive- and the negative-deflection-angle components, $\sigma_+(\theta)$ and $\sigma_-(\theta)$, are derived by using the envelopes and are shown in Fig. 2(b). The envelope uncertainties are propagated to $\sigma_\pm(\theta)$. The uncertainties in $\sigma_\pm(\theta)$ are also represented by the regions delimited by dotted lines. For comparison, the

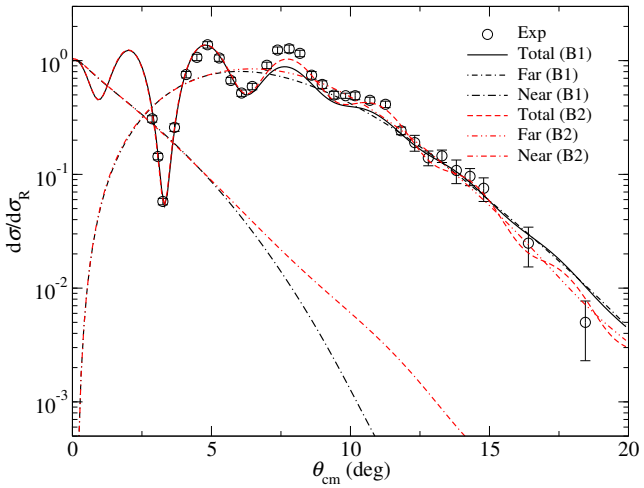

Fig. 3. Elastic scattering of ^{12}C+^{12}C at 1016 MeV. The circles represent the experimental data. The curves are the results of the optical model and nearside/farside decomposition calculations with different potentials.

nearside and farside angular distributions, $\sigma_n(\theta)$ and $\sigma_f(\theta)$, are also plotted. It can be observed that $\sigma_+(\theta)$ matches $\sigma_n(\theta)$ well with small uncertainties. Moreover, $\sigma_-(\theta)$ is close to the magnitude of $\sigma_f(\theta)$. As the calculated $\sigma_n(\theta)$ with potentials A1 and A2 are significantly close to each other, it is not feasible to determine which is closer to the derived $\sigma_+(\theta)$. However, the calculated $\sigma_f(\theta)$ with potentials A1 and A2 are evidently different. However, the relatively small values (less than 10^{-3}) of $\sigma_-(\theta)$ probably make its apparent structure meaningless [28]. In addition, the relative error of $\sigma_-(\theta)$ is significantly larger than that of $\sigma_+(\theta)$, which is consistent with the results calculated in Ref. [30], in which the author found that slight adjustments of envelopes visibly affect the

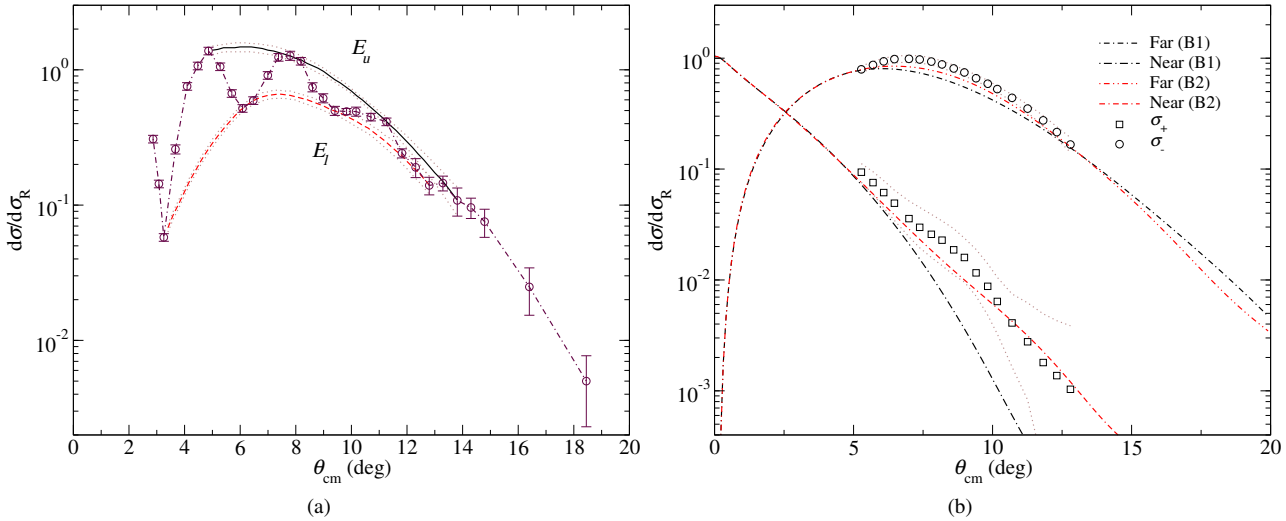

Fig. 4. Elastic scattering of ^{12}C+^{12}C at 1016 MeV: a) envelopes of the experimental data; (b) greater/smaller components in comparison with the nearside/farside components.

smaller ones of $\sigma_+(\theta)$ and $\sigma_-(\theta)$ but have little effect on the larger one. These difficulties render it impractical to determine whether $\sigma_f(\theta)$ is closer to $\sigma_-(\theta)$. Hence, the envelope method is unsuitable for resolving the refractive or diffractive potential ambiguity problem of ^{16}O+^{28}Si at 215.2 MeV.

B. ^{12}C+^{12}C at 1016 MeV

For the elastic scattering of ^{12}C+^{12}C at 1016 MeV, the calculated total, nearside and farside angular distributions with the B1 and B2 potentials are plotted in Fig. 3 in comparison with the experimental data. For the B1 potential, although the depth of the real part is smaller than that of the imaginary part, it is not a diffractive potential because it produces a Fraunhofer crossover [10]. Similar to the A1 potential, the B1 potential is a "surface transparent" one with $R_{\rm R} > R_{\rm I}$. The strength of the real part is greater than that of the imaginary part for $r \geq 2$ fm, and there is a strongly absorbing core at small radii [11]. The B2 potential is a refractive deep-V potential, similar to the A2 potential. In these calculations, following the procedure described in Ref. [11], the relativistic effects were considered by using an effective center-of-mass energy of 496.84 MeV and an effective mass of 12.27 u for ^{12}C. Observing Fig. 3, both the B1 and B2 potentials effectively reproduce the experimental data. The farside components $\sigma_f(\theta)$ are significantly close to each other in the angular range of the experimental data. However, the nearside components $\sigma_n(\theta)$ exhibit an evident difference in slope after approximately 5° in the center-of-mass system, in which $\sigma_n(\theta)$ corresponding to the B1 potential becomes smaller than that corresponding to B2.

The upper and lower envelopes are drawn for the experimental data in Fig. 4(a), and the corresponding derived $\sigma_\pm(\theta)$ are drawn in Fig. 4(b) in comparison with $\sigma_{n/f}(\theta)$. As in the case of ^{16}O+^{28}Si, the envelope uncertainties are also considered and propagated into $\sigma_\pm(\theta)$. It can be observed that $\sigma_-(\theta)$ matches $\sigma_f(\theta)$, and $\sigma_+(\theta)$ is close to $\sigma_n(\theta)$ for both B1 and B2 potentials. In this case, because the farside scattering components $\sigma_f(\theta)$ corresponding to the two potential sets are close to each other, it is not feasible to determine which one is closer to the derived $\sigma_-(\theta)$. However, the evident difference between the calculated $\sigma_n(\theta)$ with the two potential sets enables the selection of the physical potential. As for the obtained $\sigma_+(\theta)$, its magnitude is larger than 10^{-3} at almost all the scattering angles covered by the envelopes. In addition, the relative error increases as the scattering angle increases. Clearly, $\sigma_+(\theta)$ matches better with the B2 nearside component than with the B1 component. This reveals that the B2 potential is more physical, which is consistent with the results of the combined analyses of elastic scattering and the transfer reaction of ^{12}C+^{12}C at 1016 MeV in Ref. [11].

C. Factors influencing the application of the envelope method

The calculated results for ^{12}C+^{12}C at 1016 MeV preliminarily indicate the possibility of using the envelope method to address the potential ambiguity problem. Several factors influencing the application of the envelope method to potential ambiguity problems were identified.

The primary factor is the difference between the calculated $\sigma_{n/f}(\theta)$ corresponding to different potential families. If they show evident differences in $\sigma_n(\theta)$ and/or $\sigma_f(\theta)$, there is a possibility of selecting a physical potential. However, when the calculated $\sigma_{n/f}(\theta)$ values are nearly identical for different potential families, applying this method is not feasible.

The second factor is the magnitude of the smaller part of $\sigma_\pm(\theta)$. When the calculated $\sigma_{n/f}(\theta)$ exhibits evident differences from the smaller values, as in the cases of ^{16}O+^{28}Si at 251.2 MeV and ^{12}C+^{12}C at 1016 MeV, the magnitudes should not be significantly small. The present calculations

show that when the magnitudes are smaller than approximately 10^{-3}, a comparison between the smaller parts of $\sigma_{\pm}(\theta)$ and $\sigma_{n/f}(\theta)$ can provide limited information. In this case, although the derived $\sigma_{\pm}(\theta)$ matches the calculated $\sigma_{n/f}(\theta)$ well on the order of magnitude, the details of the structure become meaningless. This phenomenon was observed in the positive-/negative-deflection-angle decomposition of the inelastic scattering angular distributions using the envelope method in Ref. [28].

Furthermore, the data quality also influences the application of the envelope method. The plot of the envelopes requires well-defined maxima and minima; in other words, it requires good angular resolution. The errors of the differential cross sections should be small as they are propagated to the derived $\sigma_{\pm}(\theta)$.

Apart from the factors encountered and mentioned above, it should be noted that the Fraunhofer crossover can also influence the application. In fact, at the Fraunhofer crossover angle, the values of $\sigma_{+}(\theta)$ and $\sigma_{-}(\theta)$ should equal with each other in principle, which implies that the value of the lower envelope should be zero (cf. Eq. (5)). However, the lower envelope does not have zero points. Therefore, as indicated in Ref. [30], the data near the Fraunhofer crossover are unsuitable for use in the envelope method.

IV. SUMMARY

In this study, a trial application of the envelope method to the optical potential ambiguity problem is presented. The colliding systems of ^{16}O+^{28}Si at 215.2 MeV and ^{12}C+^{12}C at 1016 MeV were used as examples in the application. Based on the envelope method, the experimental data of the elastic scattering angular distributions were decomposed into positive- and negative-deflection-angle components (denoted as $\sigma_{+}(\theta)$ and $\sigma_{-}(\theta)$, respectively). Although the original version of the envelope method does not quantitatively consider uncertainties, the present work propagates the uncertainties of the experimental data points that determine the envelopes into the derived $\sigma_{\pm}(\theta)$. For each colliding system, the optical model and the nearside/farside decomposition calculations are performed with two potential sets, of which one is "surface tranparent" and another is refractive. For each potential set, the corresponding nearside and farside scattering components (denoted as $\sigma_n(\theta)$ and $\sigma_f(\theta)$, respectively) were compared with the derived $\sigma_{+}(\theta)$ and $\sigma_{-}(\theta)$, respectively.

For ^{16}O+^{28}Si at 215.2 MeV, the envelope method provides good estimations of $\sigma_{n/f}(\theta)$ on the order of magnitude. The nearside components $\sigma_n(\theta)$ corresponding to two potential sets are nearly identical in the angular region of the envelopes. Therefore, although the derived $\sigma_{+}(\theta)$ matches them well, it is not feasible to select a physical potential by comparing $\sigma_{+}(\theta)$ with $\sigma_n(\theta)$. By contrast, the farside components $\sigma_f(\theta)$ corresponding to two potential sets, exhibit evident differences in the angular region of the envelopes. However, the derived $\sigma_{-}(\theta)$ has small magnitudes with large uncertainties, making its structure meaningless. It is impractical to select the physical potential by comparing $\sigma_{-}(\theta)$ with $\sigma_f(\theta)$ quantitatively.

For ^{12}C+^{12}C at 1016 MeV, the derived $\sigma_{+}(\theta)$ and $\sigma_{-}(\theta)$ match the calculated $\sigma_n(\theta)$ and $\sigma_f(\theta)$ well, respectively. In this case, the farside components $\sigma_f(\theta)$ corresponding to two potential sets are significantly close to each other in the angular region of the envelopes. Although the derived $\sigma_{-}(\theta)$ matches well with $\sigma_f(\theta)$, it is not feasible to select the physical potential by comparing $\sigma_{-}(\theta)$ with $\sigma_f(\theta)$. For $\sigma_n(\theta)$, the two potential sets yield significantly different results. The calculated $\sigma_n(\theta)$ corresponding to the "surface transparent" potential B1 shows an evident smaller values after 5° in comparison with that corresponding to the refractive potential B2. The derived $\sigma_{+}(\theta)$ clearly matches much better with $\sigma_n(\theta)$ corresponding to B2. Hence, the refractive potential B2 was selected as the physical potential, which was consistent with the results given in Ref. [11].

Several factors that influence the application of the envelope method to the potential ambiguity problem were identified. We believe that one can try to use the envelope method to analyze the potential ambiguity problem when the following conditions are met: (1) the calculated $\sigma_{n/f}(\theta)$ of potential families exhibit evident differences; (2) the smaller part of $\sigma_{\pm}(\theta)$ is not too small (e.g. larger than 10^{-3}); (3) the experimental data have good angular resolutions and small errors of differential cross sections; (4) the main part of the envelopes is not close to the Fraunhofer crossover point. The envelope method has shown potential for analyzing the potential ambiguity problem. Further applications of the envelope method to the potential ambiguity problem are required to verify the method.

[1] M.E. Brandan, G.R. Satchler, The interaction between light heavy-ions and what it tells us. Phys. Rep. **285**, 143–243 (1997). doi: 10.1016/S0370-1573(96)00048-8

[2] H.R. Guo, Y.L. Han, C.H. Cai et al., Theoretical calculation and evaluation of n+^{240,242,244}Pu reactions. Nucl. Sci. Tech. **30**, 13 (2019). doi: 10.1007/s41365-018-0533-7

[3] F.F. Duan, Y.Y. Yang, J. Lei et al., Elastic scattering and breakup reactions of neutron-rich nucleus ^{11}Be on ^{208}Pb at 210 MeV. Phys. Rev. C **105**, 034602 (2022). doi: 10.1103/PhysRevC.105.034602

[4] Y.Y. Yang, X. Liu, D.Y. Pang et al., Elastic scattering of the proton drip line nuclei ^{7}Be, ^{8}B, and ^{9}C on a lead target at energies around three times the Coulomb barriers. Phys. Rev. C **98**, 044608 (2018). doi: 10.1103/PhysRevC.98.044608

[5] G. Yang, D.Y. Pang, Y.Y Yang et al., Systematic single-folding model nucleus-nucleus potential for peripheral collisions. Phys. Rev. C **107**, 044603 (2023). doi: 10.1103/PhysRevC.107.044603

[6] G. Igo, Optical-model analysis of excitation function data and theoretical reaction cross sections for alpha particles. Phys.

Rev. **115**, 1665–1674 (1959). doi: 10.1103/PhysRev.115.1665
[7] R.M. Drisko, G.R. Satchler, R.H. Bassel, Ambiguities in the optical potential for strongly absorbed projectiles. Phys. Lett. **5**, 347–350 (1963). doi: 10.1016/S0375-9601(63)94801-1
[8] M.E. Cage, A.J. Cole, G.J. Pyle, Ambiguities and systematics in the real central part of the optical-model potential. Nucl. Phys. A **201**, 418–432 (1973). doi: 10.1016/0375-9474(73)90075-4
[9] G.R. Satchler, ^{16}O+^{28}Si: Deep or shallow potentials? Nucl. Phys. A **279**, 493–501 (1977). doi: 10.1016/0375-9474(77)90582-6
[10] M.S. Hussein, K.W. McVoy, Nearside and farside: The optics of heavy ion elastic scattering. Prog. Part. Nucl. Phys. **12**, 103–170 (1984). doi: 10.1016/0146-6410(84)90003-6
[11] G.R. Satchler, Transfer reactions and optical potential ambiguities for light heavy-ion systems. Nucl. Phys. A **505**, 103–122 (1989). doi: 10.1016/0375-9474(89)90418-1
[12] W.J. Kong, D.Y. Pang, Theoretical uncertainties of (d,^{3}He) and (^{3}He,d) reactions owing to the uncertainties of optical model potentials. Nucl. Sci. Tech. **34**, 95 (2023). doi: 10.1007/s41365-023-01242-y
[13] G.B. King, A.E. Lovell, F.M. Nunes, Uncertainty quantification due to optical potentials in models for (d, p) reactions. Phys. Rev. C **98**, 044623 (2018). doi: 10.1103/PhysRevC.98.044623
[14] X.Y. Yun, D.Y. Pang, Y.P. Xu et al., What kind of optical model potentials should be used for deuteron stripping reactions? Sci. China Phys. Mech. Astron. **63**, 222011 (2020). doi: 10.1007/s11433-019-9389-6
[15] D.T. Khoa, L.H. Chien, D.C. Cuong et al., Mean-field description of heavy-ion scattering at low energies and fusion. Nucl. Sci. Tech. **29**, 183 (2018). doi: 10.1007/s41365-018-0517-7
[16] H. An, C. Cai, Global deuteron optical model potential for the energy range up to 183 MeV. Phys. Rev. C **73**, 054605 (2006). doi: 10.1103/PhysRevC.73.054605
[17] X. Li, C. Liang, C. Cai, Global triton optical model potential. Nucl. Phys. A **789**, 103–113 (2007). doi: 10.1016/j.nuclphysa.2007.03.004
[18] Y. Kucuk, I. Boztosun, T. Topel, Global optical potential for the elastic scattering of ^{6}He at low energies. Phys. Rev. C **80**, 054602 (2009). doi: 10.1103/PhysRevC.80.054602
[19] X.H. Li, L.W. Chen, Isospin dependent global neutron–nucleus optical model potential. Nucl. Phys. A **874**, 62–80 (2012). doi: 10.1016/j.nuclphysa.2011.10.008
[20] D.Y. Pang, W.M. Dean, A.M. Mukhamedzhanov, Optical model potential of A=3 projectiles for 1p-shell nuclei. Phys. Rev. C **91**, 024611 (2015). doi: 10.1103/PhysRevC.91.024611
[21] Y. Xu, Y. Han, J. Hu et al., ^{6}Li global phenomenological optical model potential. Phys. Rev. C **98**, 024619 (2018). doi: 10.1103/PhysRevC.98.024619
[22] Y. Xu, Y. Han, J. Hu et al., Global phenomenological optical model potential for the ^{7}Li projectile nucleus. Phys. Rev. C **97**, 014615 (2018). doi: 10.1103/PhysRevC.97.014615
[23] Y. Xu, X. Su, Y. Han et al., Optical potential for the elastic scattering of ^{6}Li projectile on 1p-shell nuclei. Int. J. Mod. Phys. E **31**, 2250093 (2022). doi: 10.1142/S0218301322500938
[24] Y. Han, Y. Xu, H. Liang et al., Global phenomenological optical model potential of nucleon-actinide reaction for energies up to 300 MeV. Phys. Rev. C **81**, 024616 (2010). doi: 10.1103/PhysRevC.81.024616
[25] Y. Han, Y. Shi, Q. Shen, Deuteron global optical model potential for energies up to 200 MeV. Phys. Rev. C **74**, 044615 (2006). doi: 10.1103/PhysRevC.74.044615
[26] Y.L. Xu, H.R. Guo, Y.L. Han et al., Helium-3 global optical model potential with energies below 250 MeV. Sci. China Phys. Mech. Astron. **54**, 2005 (2011). doi: 10.1007/s11433-011-4488-5
[27] R. da Silveira, Ch. Leclercq-Willain, On the separation of the nuclear and Coulomb rainbow components from the elastic scattering data. Z. Phys. A: At. Nucl. **314**, 63–67 (1983). doi: 10.1007/BF01411831
[28] R. da Silveira, Ch. Leclercq-Willain, A refractive phase relation in light-composite-particle-nucleus elastic and inelastic scattering at intermediate energies. J. Phys. G: Nucl. Phys. **10**, L157–L162 (1984). doi: 10.1088/0305-4616/10/7/002
[29] H.M. Khalil, K.W. McVoy, M.M. Shalaby, Nuclear rainbows ≡ overlapping resonances. Nucl. Phys. A **455**, 100–117 (1986). doi: 10.1016/0375-9474(86)90345-3
[30] M. Lassaut, Microscopic optical-model analysis of α-^{40}Ca elastic scattering at 104 MeV through the near/far decomposition. Nucl. Phys. A **442**, 1–16 (1985). doi: 10.1016/0375-9474(85)90129-0
[31] R.C Fuller, Qualitative behavior of heavy-ion elastic scattering angular distributions. Phys. Rev. C **12**, 1561–1574 (1975). doi: 10.1103/PhysRevC.12.1561
[32] M.H. Cha, NearFar: A computer program for near-side–farside decomposition of heavy-ion elastic scattering amplitude. Comput. Phys. Commun. **176**, 318–325 (2007). doi: 10.1016/j.cpc.2006.10.008
[33] D.M. Brink, *Semi-Classical Methods for Nucleus-Nucleus Scattering*. (Cambridge University Press, Cambridge, 1983), pp. 68–71.
[34] R. Brun, F. Rademakers, ROOT – An object oriented data analysis framework. Nucl. Instrum. Meth. A **389**, 81–86 (1997). doi: 10.1016/S0168-9002(97)00048-X
[35] I.J. Thompson, Coupled reaction channels calculations in nuclear physics. Comput. Phys. Rep. **7**, 167–212 (1988). 10.1016/0167-7977(88)90005-6
[36] J.G. Cramer, R.M. DeVries, D.A. Goldberg et al., "Unique" energy-independent Woods-Saxon optical potential for ^{16}O+^{28}Si elastic scattering. Phys. Rev. C **14**, 2158–2161 (1976). doi: 10.1103/PhysRevC.14.2158
[37] M. Buenerd, A. Lounis, J. Chauvin et al., Elastic and inelastic scattering of carbon ions at intermediate energies. Nucl. Phys. A **424**, 313–334 (1984). doi: 10.1016/0375-9474(84)90186-6
[38] G.R. Satchler, M.L. Halbert, N.M. Clarke et al., Heavy-ion elastic scattering (II). 142 MeV ^{16}O on ^{28}Si, ^{59}Co and ^{60}Ni. Nucl. Phys. A **298**, 313–332 (1978). doi: 10.1016/0375-9474(78)90259-2
[39] R. Suzuki, A. Makinaga, M. Aikawa, in *Proceedings of the 2014 symposium on nuclear data*, Hokkaido University, Sapporo, 2014, ed. by S. Ebata, S. Nakamura, S. Nakamura, H. Koura
[40] A.V. Karpov, A.S. Denikin, M.A. Naumenko et al., NRV web knowledge base on low-energy nuclear physics. Nucl. Instrum. Meth. A **859**, 112–124 (2017). doi: 10.1016/j.nima.2017.01.069